Non-linear dynamics of multimode semiconductor lasers: dispersion-based phase instability and route to single-frequency operation

Baptiste Chomet, Nathan Vigne, Grégoire Beaudoin, Konstantinos Pantzas, Stéphane Blin, Isabelle Sagnes, Stéphane Denet, Arnaud Garnache

Optics Letters

Non-linear dynamics of multimode semiconductor lasers: dispersion-based phase instability and route to single-frequency operation

Baptiste Chomet,[1,2,*] Nathan Vigne,[1] Grégoire Beaudoin,[3] Konstantinos Pantzas,[3] Stéphane Blin,[1] Isabelle Sagnes,[3] Stéphane Denet,[2] and Arnaud Garnache[1]

[1]IES, CNRS UMR 5214, Univ. Montpellier, Montpellier, France
[2]Innoptics, Institut d'Optique d'Aquitaine, Rue François Mitterrand, Talence, France
[3]C2N, CNRS UMR9001, Université Paris-Saclay, 91120 Palaiseau, France
*Corresponding author: email@my-email.com

Received 8 December 2022; revised 26 January 2023; accepted 10 February 2023; posted 10 February 2023; published 8 March 2023

Emission dynamics of a multimode broadband interband semiconductor laser have been investigated experimentally and theoretically. Non-linear dynamics of a III–V semiconductor quantum well surface-emitting laser reveal the existence of a modulational instability, observed in the anomalous dispersion regime. An additional unstable region arises in the normal dispersion regime, owing to carrier dynamics, and has no analogy in systems with fast gain recovery. The interplay between cavity dispersion and phase sensitive non-linearities is shown to affect the character of laser emission with phase turbulence, leading to regular self-excited oscillations of mode intensity, self-mode locking, and single-frequency emission stabilized by spectral symmetry breaking. Such physical behavior is a general phenomenon for any laser with a slow gain medium relative to the round trip time, in the absence of spatial inhomogeneities.

https://doi.org/10.1364/OL.482138

Developing lasers that are scalable to high powers while retaining their frequency purity is still a fundamental challenge of interest for applications. Any cavity supports excited states at several frequencies. To overcome such complexity, hard filtering technological solutions are possible, including intracavity filtering. However, no efficient fundamental solution has been found yet. Phase instability, better known in non-linear optics as modulational instability [1,2], has been identified as a driving mechanism for multimode operation in semiconductor lasers through the phase–amplitude coupling of a laser field provided by the linewidth enhancement factor [3–5]. In the absence of spatial inhomogeneities—known as spatial hole burning (SHB)—the latter produces the needed interplay of dispersive and non-linear effects and is inherent in any semiconductor laser. In the limit of near-threshold operation and assuming fast gain recovery, it was shown that Maxwell–Bloch equations could be reduced to the complex Ginzburg–Landau equation (CGLE), for which a vast body of literature exists [6]. While adiabatic elimination of the gain is a well known property of unipolar devices, fast relaxation is not applicable to conventional interband semiconductor lasers. It was nevertheless shown that these devices can undergo deterministic multimode dynamics [7,8]. In particular, regular switching of the optical frequency from blue to red on a frequency scale much smaller than all frequencies associated with the semiconductor material or the cavity round trip time was reported but, however, not yet fundamentally explained.

In this Letter, we investigate the single-mode instability of a continuous wave (cw) semiconductor laser where gain relaxation γ_e^{-1} takes place on a time scale longer than the cavity round trip time T ($\gamma_e T<1$). In a such system, four wave mixing (FWM) is expected to be weak, since carriers cannot follow fast oscillations of electric field intensity at T. However, by tuning the amount of cavity dispersion, we do find an unstable regime analogous to the anomalous dispersion regime of the usual CGLE [6]. We also find an additional unstable region that has no analogy in systems with instantaneous non-linearity. Such dynamics exclude Risken–Nummedal–Graham–Haken instability [9]. While the CGLE assumes the mean field approximation, here we propose a more general model, based on time delays, that is able to reproduce all the experimentally observed features, including high-order dispersion.

To study phase instability in slow gain media semiconductor lasers, we use quantum well (QW) vertical-external-cavity surface-emitting lasers (VeCSELs), which are inherently powerful in cw mode at room temperature, highly coherent (temporally, spatially, and in polarization), compact, and wavelength-flexible [10,11]. The stable standing wave cavity, shown in Fig. 1, is formed by a wavelength-thick GaAs-based gain mirror, a millimeters-long air gap, and a concave output coupler, where $T = 2\pi/\Delta\omega = 10$ ps and finesse $F = 600$. Thus, about 50 longitudinal modes are within the gain bandwidth. The laser operates in a single fundamental Gaussian eigenmode, thanks to pump mode matching, to prevent high-order transverse mode operation. Thanks to gain anisotropy, only one linear polarization eigenstate operates along the [110] crystal axis. Thus,

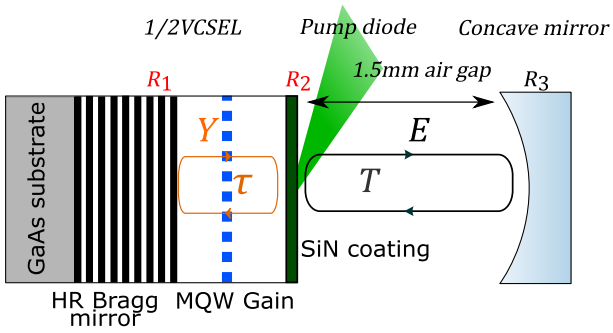

Fig. 1. VeCSEL technology in coupled-cavities configuration; τ (T) is the round trip time in the short (external) cavity, with $\tau \ll T$, $R_1 = 99.8\%$, $R_2 \simeq 0.5\%$, $R_3 = 99\%$, $R_{cc} = 10$ mm.

only non-linear longitudinal mode dynamics driven by coherent FWM and cavity phase dispersion remain possible, without any spectral and spatial inhomogeneities [10,12]. In VeCSELs, group delay dispersion is introduced through amplitude reflectivity of the microcavity (round trip time $\tau \approx 80$ fs), which acts as a Gire–Tournoi interferometer (GTI), where the coupling with the external cavity is achieved considering the reflectivity of the gain mirror's top surface (R_2) [13]. More details of the laser cavity design and dispersion calculation are provided in Supplement 1. Just above the laser threshold, the device emits a single longitudinal mode. However when the pumping level reaches a non-linear threshold, $\eta \approx 2$ (intracavity power density of ≈ 35 kW/cm^2) secondary modes start lasing. On further increasing the pumping level, many modes start oscillating.

The device was operated in either the anomalous or normal dispersion regime, exploiting tuning of the QW emission wavelength with temperature (0.2 nm/K). The top of Figure 2(a) shows the calculated group delay dispersion (GDD) introduced by the gain mirror and the bottom of Fig. 2(a) shows the laser optical spectrum acquired for different temperatures of the QW, while keeping the optical power constant at $P_{out} = 41$ mW ($\eta = 8$). With an increase of the emission wavelength, the laser light state goes from multimode to single-frequency and back to multimode again. Multimode dynamics were investigated by recording a time-resolved optical spectrum on a 10 µs time scale, corresponding to 10^6 round trips in the cavity, as shown in Fig. 2(b). Close to the zero crossing of dispersion, the dynamics are stable and the laser exhibits either single-frequency emission (III) or simultaneous emission of a few modes (II), depending on the sign of the dispersion. In both cases, intensity fluctuations [the blue curve in Fig. 2(c)] are pump noise limited below the cavity cutoff frequency $f_c = 128$ MHz, $\approx 1/(F \times T) \ll \gamma_e$. The laser then operates in class A and, slightly, class B regimes, owing to the high quality factor of the VeCSEL cavity [12]. In the anomalous dispersion regime, autocorrelation of the second-harmonic generation (SHG) [inset of Fig. 2(c)] reveals signal modulation up to 60%, with a periodicity that corresponds to $T = 10$ ps. This suggests that the formation of a highly coherent pulse train takes place in the cavity despite the absence of a saturable absorber.

When the laser operates in a more dispersive regime, either anomalous (I) or normal (IV), the dynamics are unstable but regular and deterministic [Fig. 2(b)]: the intensity of every active mode starts to oscillate in antiphase at low frequency, and the optical frequency follows a well defined sequence, progressing from the blue to the red side of the spectrum. When the reddest

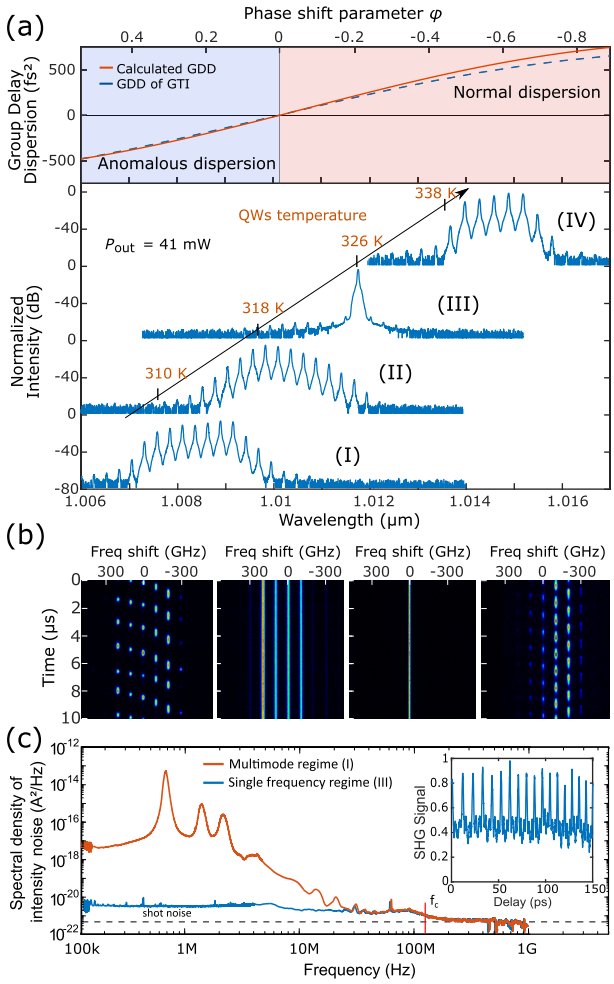

Fig. 2. (a) Top: Calculated GDD of half VeCSEL and corresponding GTI, derived from Eq. (4). Bottom: Optical spectra of VeCSEL obtained for different QW temperatures T_{qw}, where $T_{qw} = T_{peltier} + R_{th} \times P_p$ with R_{th} the thermal resistance of the half VeCSEL, estimated to be 150 K/W. (I) $P_p = 180$ mW, $T_p = 10°$C; (II) $P_p = 200$ mW, $T_p = 15°$C; (III) $P_p = 220$ mW, $T_p = 20°$C; (IV)$P_p = 270$ mW, $T_p = 30°$C. (b) Streak photographs corresponding to the optical spectra in (a). The spectral resolution is 25 GHz, which allows resolution of the longitudinal modes of the laser. (c) Intensity fluctuations in (III) single-mode and (I) multimode regimes. Inset: second-order autocorrelation measured in (II) coherent mode locked regime.

mode switches off, the sequence restarts from the bluest mode. This switching frequency appears as a peak in the intensity noise fluctuation spectrum [Fig. 2(c)] and tends to increase with the pumping power and the number of oscillating modes but stays in the 0.1–1 MHz range (see Supplement 1). Similar multimode dynamics were presented by Yacomotti *et al.* [8], but the results were explained through SHB and FWM. Conversely, even in the absence of SHB, single-mode instabilities resulting from the interplay between FWM and dispersion have been shown to occur near threshold operation [3,4]. Such explanations are not compatible with our device, where SHB is absent and multimode operation occurs at a few times the threshold power. In the following, we show that dispersion can lead to multimode emission in the presence of both phase–amplitude coupling and FWM, where carrier dynamics plays an important role.

To study the multimode dynamics of our device, we use time-delayed systems, which have been proven to correctly describe the dynamics of slow gain devices [14–16]. In particular, they do not consider small round trip losses and gain and they have shown connection with the CGLE [5]. We denote the microcavity field Y and the field in the external cavity by E, as shown in Fig. 1. Here, phase dispersion is taken into account by operating the microcavity off resonance, which acts as a detuned GTI. The resulting dimensionless rate equations for Y and the saturable gain G take the form [15]

$$\dot{Y} = \gamma_f \left(-Y + \sqrt{R_2 R(t)} e^{i\varphi} Y_\tau + \sqrt{1-R_2}\sqrt{R_3} E_T\right) \quad (1)$$

$$\dot{G} = \gamma_e \left(G_0 \eta - G - (\exp(G) - 1)|Y_\tau|^2\right) \quad (2)$$

$$E = \sqrt{1-R_2}\sqrt{R(t)} e^{i\varphi} Y_\tau - \sqrt{R_2 R_3} E_T \quad (3)$$

with $R(t) = R_1 e^{(1-i\alpha_h)G(t)}$. The subscripts T and τ denote time-delayed terms [$X_T = X(t-T)$], where the delay parameters are, respectively, the round trip time of the laser cavity and the round trip time of the GTI. The gain bandwidth of the laser is limited by the finite width of the gain spectrum γ, which is taken into account by a Lorentzian-shaped filter function with full-width at half maximum $\gamma_f = 2\gamma/\sqrt{2G_0}$. Moreover, α_h, G_0, and η represent the phase–amplitude coupling factor, the steady state gain, and the already described pump ratio over the threshold, respectively. The parameters R_1, R_2, and R_3 describe the reflectivities of the microcavity and output coupler, respectively. The coupling between E and Y is given in Eq. (3) by a delayed algebraic equation, which takes into account the multiple reflections in the external cavity. The parameter φ reflects the phase difference between photons transmitted back from the microcavity and those that are directly reflected on its top. Note that this phase shift is a function of the detuning of the photons δ_ω with respect to the microcavity mode by the relation $\delta_\omega = \varphi/\tau$. Approximating the reflection phase of the passive microcavity by a Taylor expansion close to the field carrier frequency ω_0 leads to the dispersion parameters:

$$\Phi(\omega_0)_n = \frac{\partial^n}{\partial \omega^n} \arg\left[\frac{-\sqrt{R_2} + \sqrt{R_1} e^{i\omega\tau + i\varphi}}{1 - \sqrt{R_1 R_2} e^{i\omega\tau + i\varphi}}\right]\Bigg|_{\omega=\omega_0}. \quad (4)$$

The dashed line in the top of Fig. 2(a) shows the second-order dispersion (Φ_2 = GDD) introduced by the microcavity using the parameters $R_2 = 0.0035$ and $\tau = 80$ fs, which reproduces well the calculated GDD of the half VeCSEL. Our model also includes all high orders of dispersion. In the following simulations, the laser operating frequency is set to $\omega_0 = 0$ and the parameter φ is used to tune the resonance frequency of the microcavity, introducing the desired amount of dispersion into the external cavity.

To study the region where light is stable, stability analysis of the steady state [$E(t) = \sqrt{\eta - 1} e^{-i\alpha_h G_0 t/2T}$, $G = G_0$] is performed using the continuation package DDE-BIFTOOL, as shown in Figs. 3(a) and 3(b). The parameters $\alpha_h \mathrm{GDD}\gamma^2/G_0$ (the ratio of the cavity dispersion over diffusion) and $\gamma_e \eta T$ (carrier response time normalized to the cavity round trip) capture the stability of the system. In this parameter space, the inner region confined by the lines has stable, purely single-mode solutions, while the two outer regions exhibit multimode solutions. The parameter coordinates corresponding to our laser parameters in Fig. 2(a) are marked in Fig. 3(b) (I to IV). As light intensity is increased, instability through a Hopf bifurcation occurs along the intensity

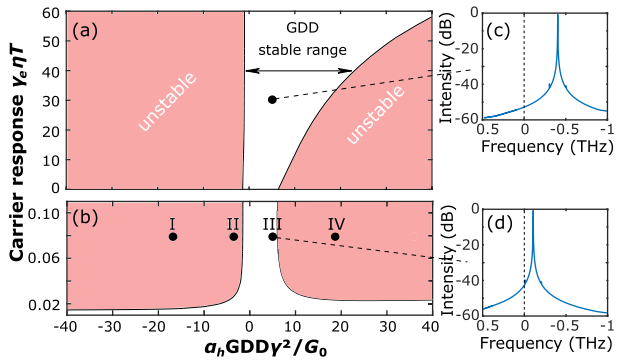

Fig. 3. Single-mode stability diagram in normalized parameter space ($\alpha_h \mathrm{GDD}\gamma^2/G_0$, $\gamma_e \eta T$). (a) Evolution of stable range of GDD as gain recovery becomes comparable to round trip time. (b) Enlargement corresponding to VeCSEL parameters. I to IV correspond to experimental situations [Fig. 2(a)]. (c, d) Spectra obtained from simulations of Eqs. (1) to (3) are shown for different points in parameter space, confirming that single-frequency operation can be achieved even at high pump power. Other simulations parameters are (γ_e, γ, T, τ, G_0, α_h, R_1, R_2, R_3) = (10^9 s^{-1}, 1.4×10^{13} s^{-1}, 10 ps, 80 fs, 0.01, 2, 1, 0.0035, 0.99).

axis when diffusion—spectral filtering—is not strong enough to compete with FWM. It is shown in Supplement 1 that the non-linear threshold for which multimode emission occurs is

$$\eta_{\mathrm{NL}} = 1 + \Delta\omega^3/\alpha_h \gamma_e \gamma^2. \quad (5)$$

Equation (5) states that, even in a slow gain medium ($\gamma_e^{-1} \gg T$), where FWM is expected to be negligible, instability of the laser emission can occur well above the laser threshold in the presence of a phase–amplitude coupling factor. According to the VeCSEL parameters, $\eta_{\mathrm{NL}} \sim 1.7$, which is about the measured value. Above this instability threshold, we find not only that there is instability in the anomalous dispersion regime, but also that the stable range of GDD is bounded from above. The range is not symmetric about zero, but is centered on the positive side of the GDD. This is again in agreement with what experiments indicate. We show in Supplement 1 that the lower bound of this range is analogous to the boundary between anomalous and normal dispersion in the CGLE, where the necessary condition is obtained for GDD$< -G_0/\alpha_h\gamma^2 \approx -25\,\mathrm{fs}^2$. As for the upper bounds, we found out that these result from carrier dynamics and are absent in the modulational instability results of the usual CGLE with instantaneous non-linearities [6]. This is shown in Fig. 3(a), where the stable range of GDD increases with a large increase of the light intensity. In the limit where $1/T\gamma_e\eta \to 0$, as is the case for lasers with fast gain or instantaneous non-linearity instability in the normal dispersion regime disappears. Figure 3(b) shows the light stability region corresponding to the VeCSEL parameters. In the stable regime, simulation of the laser dynamics confirms the stability analysis results, which predict that no instability will occur, and hence the emission of a single frequency [Fig. 3(c,d)]. Notice, however, that the laser will rather operate on the *red* side of the gain spectrum and this redshift will increase with respect to the pumping power. Thus, in the presence of both GDD>0 and strong phase–amplitude coupling, emission of the laser in stable configurations is characterized by a *non-linear redshift* of its optical frequency.

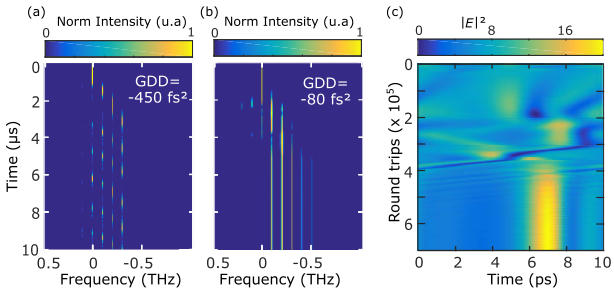

Fig. 4. Numerical simulation of spectrotemporal dynamics of laser emission for different phase shift φ of GTI. Corresponding values of GDD are indicated above; $\eta = 8$, and other parameters are the same as in Fig. 3. (a) $\varphi = 0.5$. (b) $\varphi = 0.08$. (c) For the latter, space time representation of the laser intensity $|E|^2$ over 700 000 round trips in the cavity.

In the unstable regions, the non-linear multimode dynamics of the laser emission were investigated through numerical integration of Eqs. (1) to (3). The ratio between cavity dispersion and FWM is shown to affect the character of the laser emission (Supplement 1). When dispersion dominates over non-linearity, the optical frequency tends to be chirped in one direction or another, away from the gain peak. Here it is FWM, through the alpha factor, that induces an enhancement of the gain for longer wavelengths and results in a jump from one longitudinal mode to another, located in the red side of the spectrum [8,17]. This leads to a progression from blue to red until the FWM gain cannot compensate for the losses due to spectral filtering, which results in a jump of the optical frequency to the gain peak. These dynamics are illustrated in Fig. 4(a), which shows the spectrotemporal traces of the laser emission when the GTI introduces an amount of GDD = $-450\,\mathrm{fs}^2$. In good agreement with the experimental trace [Regime I in Fig. 2(b)], simulations reveal around five optical modes whose intensity oscillates every $N \times t_c \sim 1.5\,\mu\mathrm{s}$, where N is the number of oscillating modes and $t_c = (2\pi)^2/G_0\alpha_h\gamma_e(\eta - 1)$ (Supplement 1). Similar dynamics were obtained in the normal dispersion regime for GDD = $+450\,\mathrm{fs}^2$.

If non-linearity dominates, a variety of dynamic regimes is possible. For example, the spectrotemporal trace shown in Fig. 4(b) reveals the existence of a mode locking regime close to the line of instability in the anomalous dispersion regime [Regime (II) in Fig. 3]. Its space–time representation [Fig. 4(c)] shows the temporal evolution of the laser intensity according to the number of round trips. After a relatively long time interval (about 500 000 round trips), the laser reaches a frequency comb regime, where a single pulse is stabilized in the cavity, in good agreement with the SHG measurements. Close to resonance, ϕ_2 becomes small and ϕ_3 (third-order dispersion) becomes dominant. Although we have checked that a finite amount of GDD is necessary to trigger instability, higher-order terms do play a role in stabilizing the pulse in the cavity. Investigating their role in the dynamics would be part of future work.

In conclusion, we investigated the impact of phase dispersion on the non-linear multimode dynamics of a quantum well interband semiconductor laser. While here the carrier lifetime well exceeds the round trip time ($\gamma_e^{-1} \gg T$), FWM in the presence of phase–amplitude coupling leads to phase instability and turbulence of the laser emission. In contrast with the usual modulational instability results of the CGLE, which occurs only in the anomalous dispersion regime, here we found an additional unstable region that arises as a result of carrier dynamics, and has no analogy in systems with an instantaneous non-linearity. The analysis of the multimode dynamics reveals the existence of regular but unstable dynamics that lead the optical frequency to chirp from the blue to the red side of the spectrum. Such dynamics have been reported in semiconductor lasers [7,8,18] or dye lasers [19], all systems whose carrier lifetime exceeds the round trip time ($\gamma_e^{-1} \geq T$), with strong phase–amplitude coupling. Finally, strongly stable single-frequency non-linear laser emission arises as the laser breaks spectral symmetry to oscillate on the red side of the gain spectrum, even at high intracavity power (~MW/cm^2).

Funding. Association Nationale de la Recherche et de la Technologie (BLASON, STAE MUSE, TAPAS); Agence Nationale de la Recherche.

Acknowledgments. The authors acknowledge French RENATECH network and the Agence Nationale de la Recherche (ANR-18-CE24-BLASON, ANR-19-CE24-SPATIOTERA, ANR-16-ASTR-TAPAS), ANRT, MUSE-STAE. The authors thank Mikhaël Myara (IES) for his help in noise measurements, J. Javaloyes (UIB) and A. Vladimirov (WIAS) for fruitful discussions on DDE.

Disclosures. The authors declare no conflicts of interest.

Data availability. Data underlying the results presented in this paper are not publicly available at this time but may be obtained from the authors upon reasonable request.

Supplemental document. See Supplement 1 for supporting content.

REFERENCES

1. G. P.Agrawal, Nonlinear fiber optics (Elsevier, 2007).
2. T. J. Kippenberg, A. L. Gaeta, M. Lipson, and M. L. Gorodetsky, Science **361**, eaan8083 (2018).
3. L. Gil and G. L. Lippi, Phys. Rev. A **90**, 053838 (2014).
4. M. Piccardo, B. Schwarz, D. Kazakov, M. Beiser, N. Opacak, Y. Wang, S. Jha, J. Hillbrand, M. Tamagnone, W. T. Chen, A. Y. Zhu, L. L. Columbo, A. Belyanin, and F. Capasso, Nature **582**, 360 (2020).
5. A. Pimenov, S. Slepneva, G. Huyet, and A. G. Vladimirov, Phys. Rev. Lett. **118**, 193901 (2017).
6. I. S. Aranson and L. Kramer, Rev. Mod. Phys. **74**, 99 (2002).
7. L. Furfaro, F. Pedaci, M. Giudici, X. Hachair, J. Tredicce, and S. Balle, IEEE J. Quantum Electron. **40**, 1365 (2004).
8. A. M. Yacomotti, L. Furfaro, X. Hachair, F. Pedaci, M. Giudici, J. Tredicce, J. Javaloyes, S. Balle, E. A. Viktorov, and P. Mandel, Phys. Rev. A **69**, 053816 (2004).
9. H. Risken and K. Nummedal, J. Appl. Phys. **39**, 4662 (1968).
10. A. Laurain, M. Myara, G. Beaudoin, I. Sagnes, and A. Garnache, Opt. Express **18**, 14627 (2010).
11. B. Chomet, J. Zhao, L. Ferrieres, M. Myara, G. Guiraud, G. Beaudoin, V. Lecocq, I. Sagnes, N. Traynor, G. Santarelli, S. Denet, and A. Garnache, Appl. Opt. **57**, 5224 (2018).
12. A. Garnache, A. Ouvrard, and D. Romanini, Opt. Express **15**, 9403 (2007).
13. P. French, G. Chen, and W. Sibbett, Opt. Commun. **57**, 263 (1986).
14. A.G. Vladimirov and D.V. Turaev, Radiophys. Quantum Electron. **47**, 769 (2004).
15. R. M. Arkhipov and A. G. Vladimirov, Appl. Phys. B **118**, 539 (2015).
16. M. Marconi, J. Javaloyes, S. Balle, and M. Giudici, Phys. Rev. Lett. **112**, 223901 (2014).
17. A. Bogatov, P. Eliseev, and B. Sverdlov, IEEE J. Quantum Electron. **11**, 510 (1975).
18. Y. Tanguy, J. Houlihan, G. Huyet, E. A. Viktorov, and P. Mandel, Phys. Rev. Lett. **96**, 053902 (2006).
19. S. E. Vinogradov, A. A. Kachanov, S. A. Kovalenko, and É. A. Sviridenkov, Pis'ma Zh. Eksp. Teor. Fiz. **55**, 560 (1992).